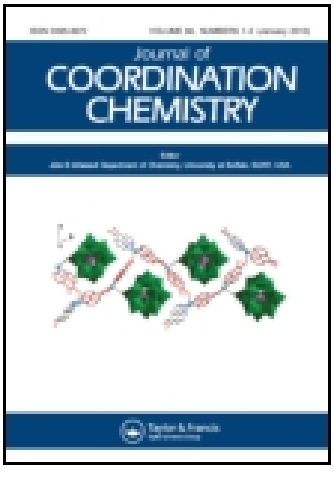

Journal of Coordination Chemistry
Publication details, including instructions for authors and subscription information:
http://www.tandfonline.com/loi/gcoo20

Aqueous complexation studies of lead(II) and cadmium(II) with 1,3-bis(tris(hydroxymethyl)methylamino)propa pH buffer

Carlos M.H. Ferreira[a], Isabel S.S. Pinto[a], Georgina M.S. Alves[a], Seyedeh Maryam Sedeghi[a] & Helena M.V.M. Soares[a]
[a] Faculdade de Engenharia, REQUIMTE - Departamento de Engenharia Química, Universidade do Porto, Porto, Portugal
Accepted author version posted online: 10 Sep 2014.Published online: 08 Oct 2014.

To cite this article: Carlos M.H. Ferreira, Isabel S.S. Pinto, Georgina M.S. Alves, Seyedeh Maryam Sedeghi & Helena M.V.M. Soares (2014) Aqueous complexation studies of lead(II) and cadmium(II) with 1,3-bis(tris(hydroxymethyl)methylamino)propane pH buffer, Journal of Coordination Chemistry, 67:20, 3354-3370, DOI: 10.1080/00958972.2014.963570

To link to this article: http://dx.doi.org/10.1080/00958972.2014.963570

Journal of Coordination Chemistry, 2014
Vol. 67, No. 20, 3354–3370, http://dx.doi.org/10.1080/00958972.2014.963570

Aqueous complexation studies of lead(II) and cadmium(II) with 1,3-bis(tris(hydroxymethyl)methylamino)propane pH buffer

CARLOS M.H. FERREIRA, ISABEL S.S. PINTO, GEORGINA M.S. ALVES, SEYEDEH MARYAM SEDEGHI and HELENA M.V.M. SOARES*

Faculdade de Engenharia, REQUIMTE – Departamento de Engenharia Química, Universidade do Porto, Porto, Portugal

(*Received 27 February 2014; accepted 1 August 2014*)

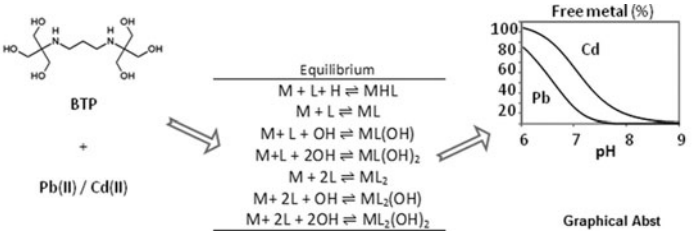

Hydrogen buffers are important in biological studies, as a steady hydrogen concentration is of great importance in most scientific studies. One of these buffers is 1,3-bis(tris(hydroxymethyl)methylamino)propane (BTP), which, considering its structure, has complexing capabilities, as previously shown for other metals. In order to know the stability constants for Cd(II) or Pb(II) with BTP, glass electrode potentiometry and direct current polarography studies were carried out. Our results show that both metals form metal complexes, with Pb(II) forming stronger complexes with BTP as evidenced by its higher stability constants. In the Pb-BTP system, five species were described; PbHL, PbL, PbL_2, $PbL_2(OH)$, and $PbL_2(OH)_2$, and their stability constants were determined to be 11.4 ± 0.3, 4.7 ± 0.3, 8.8 ± 0.2, 14.4 ± 0.3, and 18.4 ± 0.3, respectively. For the Cd-BTP system, four complexes were detected; CdHL, CdL, $CdL(OH)$, and $CdL(OH)_2$, and their stability constants were also determined as 10.9 ± 0.4, 4.10 ± 0.07, 8.2 ± 0.2, and 10.9 ± 0.2, respectively. These complexes decrease considerably the amount of free metal in solution within the buffering pH range. This fact should be considered when planning experiments were BTP and Pb(II) and/or Cd(II) ions are present.

Keywords: Biological buffer; Metal depletion; Metal complexation; Speciation simulations; Stability constants

*Corresponding author. Email: hsoares@fe.up.pt

1. Introduction

Lead [Pb(II)] and cadmium [Cd(II)] are toxic metals of great concern [1, 2]; both of them are target of regulatory legislation, like the EU's Restriction of Hazardous Substances Directive [3].

When working with biological systems, stable pH is often a requirement, as hydrogen concentration affects the rate of enzymatic reactions, stability of the biological molecules, and the overall fitness of the cell. Also, pH is responsible for the efficiency of several chemical reactions within the cell. When studying metal effects, such as of Pb(II) and Cd(II), on biological samples or carrying out speciation studies in biological media or environmental samples, it is often desirable to maintain a constant pH. For this purpose, appropriate buffer solutions are used. Good *et al.* [4] and Ferguson *et al.* [5] described several biological buffers, which are compatible with most common physiological media. Most of these buffers are zwitterionic, containing secondary or tertiary amines, hydroxyalkyl groups, and/or sulfonic groups responsible for their buffer properties [4, 5].

Among other similar buffers, 1,3-bis(tris(hydroxymethyl)methylamino)propane, also known as bis-tris propane (BTP) (figure 1), is one example of a polyamine, commercially available from Sigma–Aldrich. Its pH buffering ranges between 6.3 and 9.5. This large pH range makes BTP suitable for many applications. However, considering that this compound has two secondary amines and hydroxymethyl groups (figure 1), it is expected that BTP complexes strongly with metals in solution. In fact, previous studies have shown that BTP forms strong complexes with Ni(II), Co(II), Zn(II) [6], and Cu(II) [7] in its buffering pH range. Therefore, metal conditions can be significantly modified when BTP is used as a buffer.

As far as we know, no work concerning complexation of Cd(II) and Pb(II) with BTP is described in the literature. Formation constants of BTP complexes in aqueous solution with Cd(II) and Pb(II) were determined for the first time by glass electrode potentiometry (GEP) and direct current polarography (DCP) in an attempt to understand how BTP can alter the quantity of free metal ions in solution within its buffering pH range. Alternating current polarography (ACP) was also run, in the absence of metal ion, for evaluating the adsorption of BTP at the surface of the working mercury electrode.

2. Experimental

2.1. *Materials and instrumental conditions*

BTP (99%) was purchased from Sigma–Aldrich (St. Louis, Missouri, USA) and was used as received. A Cd(II) standard solution, 8.90×10^{-2} M, and a Pb(II) standard solution, 4.83×10^{-2} M, both from Merck, were used. A stock solution of about 0.1 M KOH was standardized with potassium hydrogen phthalate by potentiometric titration as previously

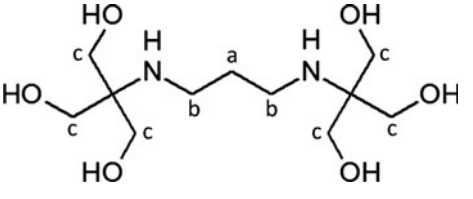

Figure 1. Chemical structure of BTP.

reported [8]. A detailed description of the remaining reagents and experimental conditions of standardization were reported previously [8].

All measurements reported in this work were carried out using solutions with ionic strength adjusted to 0.1 M KNO_3 in a Metrohm (Herisau, Switzerland) jacketed glass vessel equipped with a magnetic stirrer and thermostatted at 25 ± 0.1 °C using a water bath.

All polarographic measurements were performed in a Model 663 VA stand (Metrohm) equipped with a multimode electrode (Metrohm, model 6.2146.020) as a working electrode, set in the dropping mercury mode. A silver/silver chloride, 3 M KCl (Metrohm) and a glassy carbon electrode (Metrohm) were employed as reference and counter electrodes, respectively. The VA stand was coupled to a micro-Autolab system (Eco Chemie, Utrecht, The Netherlands) controlled by a personal computer (PC). The pH measurements were carried out with a GPL22 meter (Crison, Barcelona, Spain) with a sensitivity of ±0.1 mV (±0.001 pH units) with a combined silver/silver chloride reference electrode/glass electrode (Crison Switzerland).

Potentiometric titrations were carried out with a PC-controlled system comprised of a Crison MicroBU 2030 microburette (Barcelona, Spain) and a micropH 2002 meter with a Philips GAH110 glass electrode and an Orion 90-02-00 double-junction reference electrode. The automatic acquisition of potentiometric data was achieved by a homemade PC program, COPOTISY.

2.2. *Procedure*

2.2.1. Calibration of the glass electrode. For all techniques, prior to the experiments, the glass electrode was calibrated following a protocol previously described [8].

2.2.2. Alternating current polarography. With the objective to evaluate the adsorption of BTP on the surface of the working electrode, ACP studies were conducted. AC polarograms were run without the metal ion using experimental conditions described elsewhere [8]. The potential range used in the polarogram scans was 0.0 to −1.2 V *versus* Ag/AgCl(s), 3 M KCl, at three different pH levels: 5.0, where most BTP is in its H_2L form; 8.0, where BTP is found mostly as HL^-; and 11.0, where the ligand is found as L^{2-}. Two BTP concentrations were analyzed: 3.0×10^{-3} and 3.5×10^{-3} M; a solution of KNO_3, without BTP, was also tested. AC polarograms were run at two different phase angles: 0° and 90°. For each condition tested, scans were made until at least three measurements were in agreement.

2.2.3. Direct current polarography. The DCP titrations were performed at different total ligand to total metal concentration ratios ($[L_T] : [M_T]$) and different pH ranges. For each M-BTP system, two DCP titrations were performed for each $[L_T] : [M_T]$ ratio. For Pb-BTP system, the following $[L_T] : [Pb_T]$ ratios were used: $[L_T] : [Pb_T] = 50$ and $[L_T] : [Pb_T] = 100$, with metal concentration of 2×10^{-5} and 1×10^{-5} M, respectively, between pH 4.0 and 11.0. For Cd-BTP system, the $[L_T] : [Cd_T]$ ratios studied were as follows: $[L_T] : [Cd_T] = 300$ and $[L_T] : [Cd_T] = 350$, with a metal concentration of 1×10^{-5} M for both ratios in the pH range 4.0 and 11.0. For both M-BTP systems, the pH steps were kept at 0.1 pH units, totaling about 40–50 polarograms (representing all the species present at each pH value) recorded for each titration. A drop time of 2 s and a step potential of 8 mV were used. The equilibrium of the metal–ligand solutions was tested, and it was reached in a few minutes.

2.2.4. Glass electrode potentiometry. For the Pb-BTP system, four titrations were conducted, with constant volume additions, in the pH range 4.0 and 8.0. Two different $[L_T]:[Pb_T]$ ratios were used: $[L_T]:[Pb_T] = 4$ (one titration) and $[L_T]:[Pb_T] = 8$ (three titrations from three independent solutions) with metal concentrations of 1×10^{-3} and 5×10^{-4} M, respectively. For the Cd-BTP system, four titrations from four independent solutions were carried out, with constant volume additions, in the pH range of 3.5 and 8.5, with a $[L_T]:[Cd_T] = 4$ and a metal concentration of 1×10^{-3} M.

2.2.5. Nuclear magnetic resonance. The ^1H nuclear magnetic resonance (NMR) measurements were performed on a Bruker Avance III-400 MHz spectrophotometer for the Pb-BTP system using $[L_T]:[Pb_T] = 2$ with Pb(II) 1×10^{-4} M. Measurements were conducted in H_2O to which several drops of D_2O had been added. Previously, simulation calculations, using the final models, were conducted to define the pH values where maximum concentration of each species is formed: pH 3 and 7.5 were selected for no and observable complexation, respectively.

2.3. *Data treatment*

For the ACP data treatment, each experimental condition tested (background electrolyte solution or solutions of BTP at different concentrations and pH values), the variation of the capacitance as a function of the potential was calculated. Calculation of the capacitance–potential curves was done from the resulting current intensities, recorded as described above. From the impedance measurement data, the value of the capacitance (C) was calculated using the following equation:

$$C = \frac{-1}{Z'' \times 2 \times \pi \times f} \tag{1}$$

where Z'' is an imaginary component related to impedance and f the frequency; for further detail, see Bard and Faulkner [9].

The refinement of the polarographic data was conducted using the Cukrowski methodology, as described elsewhere [10]. The refinement uses mass-balance equations for labile (on the polarographic timescale) and reversible metal–ligand systems when studied at a fixed $[L_T]:[M_T]$ ratio and variable pH. Then, comparative analysis of the experimental and calculated complex formation curves (ECFC and CCFC, respectively) is conducted to refine the models proposed.

As refinement of the polarographic data requires curves representative of a fully reversible electrochemical process, a correction procedure was applied when necessary. For this purpose, a previously described method [11] was used in order to correct the gamma coefficient. This method corrects the semi-reversibility of the DCP data by fixing the gamma coefficient and then adjusting the limiting diffusion current and potential of half height.

For glass electrode potentiometric data, the refinement operations were conducted using the equilibrium simulation for titration analysis (ESTA) program package [12, 13]. The refinement involves solving mass-balance equations, including an equation for the total proton concentration (the species being measured with GEP) in a way that the computed free proton concentration reproduces the experimental potential in the glass electrode as accurately as possible. The use of graphic plotting of Z-bar(H) and Z-bar(M) functions resulting from the resolved equations provides help to decide more accurately the final model [12].

Table 1. Protonation constants for water and BTP and overall stability constants for lead(II) and cadmium(II) complexes with OH^- at 25 °C.

	Equilibrium	Log β	μ (M L^{-1})	Refs.
Water	$H_2O \rightleftharpoons H^+ + OH^-$	−13.78	0.1	[14]
BTP	$H^+ + L^{2-} \leftrightarrows HL^-$	9.07	0.1	[6]
	$2H^+ + L^{2-} \leftrightarrows H_2L$	15.95	0.1	[6]
Lead	$Pb^{2+} + OH^- \rightleftharpoons PbOH^+$	5.9	0.1	[14]
	$Pb^{2+} + 2OH^- \rightleftharpoons PbOH_2$	10.4	0.3	[14]
	$Pb^{2+} + 3OH^- \rightleftharpoons PbOH_3^-$	13.3	0.3	[14]
	$2Pb^{2+} + OH^- \rightleftharpoons Pb_2OH^{3+}$	7.0	1.0	[14]
	$3Pb^{2+} + 4OH^- \rightleftharpoons Pb_3OH_4^{2+}$	31.4	0.1	[14]
	$4Pb^{2+} + 4OH^- \rightleftharpoons Pb_4OH_4^{4+}$	34.9	0.1	[14]
	$6Pb^{2+} + 8OH^- \rightleftharpoons Pb_6OH_8^{4+}$	67.1	0.1	[14]
	$Pb(OH)_2(s) \rightleftarrows Pb^{2+} + 2OH^-$	−16.8	0.0	[14]
Cadmium	$Cd^{2+} + OH^- \rightleftarrows CdOH^+$	3.77	0.1	[14]
	$Cd^{2+} + 2OH^- \rightleftarrows CdOH_2$	7.10	0.1	[14]
	$Cd^{2+} + 3OH^- \rightleftarrows CdOH_3^-$	10.30	3.0	[14]
	$Cd^{2+} + 4OH^- \rightleftarrows CdOH_4^{2-}$	8.70	0.01	[14]
	$2Cd^{2+} + OH^- \rightleftarrows Cd_2OH^{3+}$	4.60	3.0	[14]
	$4Cd^{2+} + 4OH^- \rightleftarrows Cd_4OH_4^{4+}$	23.20	0.0	[14]
	$Cd(OH)_2(s) \rightleftarrows Cd^{2+} + 2OH^-$	−14.14	0.01	[14]

In both refinement operations, the water dissociation constant [14] and ligand protonation constants [6], as well as all known stability constants for $M_x(OH)_y$ [14] (table 1) species, were used in the models and kept constant.

3. Results and discussion

3.1. *Adsorption studies*

As metal stability constants, calculated by polarographic methods, require the absence of adsorption of the ligand at the mercury surface electrode, ACP experiments were performed in order to disclose the presence of such phenomena in our systems. The capacitance was then calculated for each condition and compared with the electrolyte solution. Figure 2 shows the capacitance in function of potential curves recorded at different pH values. Comparing the capacitance–potential curves recorded for the BTP concentration of 3.5×10^{-3} M with those recorded in the presence of the electrolyte only, no significant differences are observed. Based on these results, we can say that there is no adsorption of BTP at the mercury surface electrode up to 3.5×10^{-3} M for the pH values tested.

3.2. *Complexation studies of the Pb-BTP system*

From the analyses of the different DCP titrations, performed at two $[L_T] : [Pb_T]$ ratios ($[L_T] : [Pb_T] = 50$ and $[L_T] : [Pb_T] = 100$) between pH 4.0 and 11.0, only one DC wave was observed, which moved to more cathodic values. These results indicate that the Pb-BTP system behaves as a labile system throughout the titration experiments [15]. Since all titrations performed presented similar behavior, further discussion, presented below, will be focused only on one titration, $[L_T] : [Pb_T] = 100$.

From the analysis of the slopes obtained by plotting $E_{1/2}$ *versus* pH, it is possible to predict the major species present in a given pH range. When a metal species is predominant at

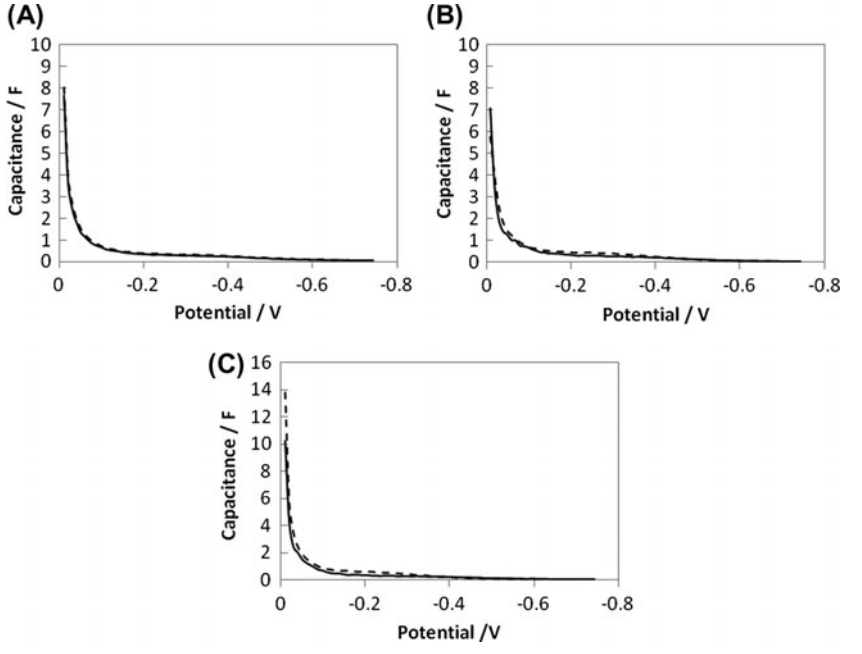

Figure 2. Capacitance in function of potential, ranging from 0.0 to −0.75 V. KNO_3 0.1 M solutions without any buffer (solid line) or with BTP buffer (dashed line, [BTP] = 3.5×10^{-3} M) for pH 5 (A), pH 8 (B), and pH 11 (C).

a given pH, a slope of $m \times (-59.16) \times n^{-1}$ should be observed (m and n stand for the number of protons and electrons involved in the electrochemical reaction, respectively) [10]. Based on this principle, three different regions can be outlined in figure 3(A). Region I is for pH values below 7, where no relevant shift of $E_{1/2}$ was found, showing that no complexation occurred up to pH 7. In region II, a slope of −23.1 mV per pH unit is found, which is close to the value of −29.6 mV per pH unit, characteristic of the involvement of one proton in the electrochemical reaction at the mercury drop electrode. Given that in the considered pH range (7.0–8.2), most of the ligand is in the HL form and a small quantity remains as H_2L, the following reactions may be considered (charges were omitted for simplicity):

$$ML + H + 2e \rightleftharpoons M(Hg) + HL \tag{2}$$

$$MHL + H + 2e \rightleftharpoons M(Hg) + H_2L \tag{3}$$

A thorough analysis of figure 3(A) shows that the transition from zone I to zone II is gradual, as at pH 7, a slight change in the potential is already visible. This may indicate the presence of PbHL, according to reaction 3. Because, at this pH range, HL^- is the major form of the ligand, the formation of PbL is expected according to reaction 2. Nevertheless, as the slope does not reach the theoretical value (−29.6 mV per pH unit), probably none of the species is present isolated and/or in full extension, but a mixture of the mentioned species is expected in this pH range. In zone III (pH 8.3–10.9), a slope of −52.8 mV per pH

unit is observed; this value is close to the theoretical slope (−59.2 mV per pH unit) typical of reactions with two protons. Part of zone III occurs at pH values below the pKa_2, which means that HL^- is still the major form of the ligand. Therefore, the following reactions must be considered:

$$ML_2 + 2H + 2e \rightleftharpoons M(Hg) + 2HL \quad (4)$$

$$ML(OH) + 2H + 2e \rightleftharpoons M(Hg) + HL + H_2O \quad (5)$$

$$M(OH)_2 + 2H + 2e \rightleftharpoons M(Hg) + 2H_2O \quad (6)$$

During the experiments, no precipitation was observed up to pH 10.9, so $Pb(OH)_2$ should not be considered as a major species.

For pH values above pKa_2, the ligand is mostly in its deprotonated form (L^{2-}) and, consequently, different reactions might take place at the mercury drop electrode:

$$ML_x(OH)_y + yH + 2e \rightleftharpoons M(Hg) + xL + yH_2O \quad (7)$$

Once the ligand is fully deprotonated, the amount of protons involved, and therefore the slope, is only related with the number of hydroxide groups in the complex.

By analyzing the $E_{1/2}$ *versus* pL plot [figure 3(B)], it is possible to study the formation of the PbL_x species [16]. In figure 3(B), two distinct zones in the curve can be identified, with slopes of −23.6 and −66.6 mV per pL unit, respectively; these slopes support the formation of PbL and PbL_2. Again, the slope that indicates the formation of PbL is lower than the theoretical Nernstian slope, which points toward a minor quantity of this species in the pH range 7.3–8.0.

The graphic analysis described above indicates that the model that better explains the experimental results is one including $PbL_xH(OH)_y$ species (x = 1, 2; y = 0, 1, 2). The following models were refined in order to fit the experimental data:

(1) PbL, PbL_2, $PbL_2(OH)$, and $PbL_2(OH)_2$
(2) PbHL, PbL, PbL_2, $PbL_2(OH)$, and $PbL_2(OH)_2$

Optimization and refinement of the stability constants of the Pb-BTP system were performed using the ECF and CCF curves (figure 4). Table 2 shows the refined stability constants for $[L_T] : [Pb_T] = 100$ assuming the two models mentioned above. Model II was able to fit consistently better than model I as a lower global standard deviation error was always obtained (table 2). This small change is inherent to the introduction of PbHL in the model, which slightly changes the adjustment of CCFC between pH 6.0 and 7.3 [see enlargement in figure 4(A)]. Although the fitting was better when PbHL was included, the refined stability constants for the other species are almost the same for the two models, indicating that even if formed, the quantity of PbHL should be minor. For comparative purposes, a CCFC for the model containing only lead hydroxide complexes was added to the graph to further corroborate the formation of PbL_xOH_y species. The difference between the ECFC [unfilled dots in figure 4(A)] and the CCFC for the $Pb_x(OH)_y$ species alone [small filled dots in figure 4(A)] clearly shows that $PbL_x(OH)_y$ species are formed throughout the pH range indicated. This figure also shows that in the absence of BTP complexation, precipitation of

Table 2. Refinement of the stability constants (as $\log_{10} \beta$) for the Pb-BTP system determined by DCP and GEP at 25 °C and ionic strength of 0.1 M KNO_3.

	DCP					GEP		
$[L_T] : [Pb_T]$	100		100	50	50	4		8
$[Pb_T]$ (M)	1×10^{-5}		1×10^{-5}	2×10^{-5}	2×10^{-5}	1×10^{-3}		5×10^{-4}
complex	Model I	Model II	Model II	Model II	Model II	Model I	Model II	Model II
PbHL	NI	11.4 ± 0.3	11.2 ± 0.3	11.5 ± 0.1	11.72 ± 0.08	NI	11.12 ± 0.09	11.2 ± 0.1
PbL	4.90 ± 0.04	4.82 ± 0.07	4.2 ± 0.2	4.92 (fixed)	4.97 (fixed)	4.97 ± 0.02	4.93 ± 0.02	4.91 ± 0.03
PbL_2	8.81 ± 0.07	8.87 ± 0.08	8.5 ± 0.1	9.04 ± 0.05	8.94 ± 0.06	8.34 ± 0.09	8.54 ± 0.05	8.50 ± 0.09
$PbL_2(OH)$	14.27 ± 0.02	14.26 ± 0.02	14.03 ± 0.03	14.50 ± 0.02	14.69 ± 0.02	NI	NI	NI
$PbL_2(OH)_2$	18.03 ± 0.02	18.04 ± 0.01	18.19 ± 0.01	18.54 ± 0.01	18.63 ± 0.01	NI	NI	NI
pH range	4.6–11.0	4.6–11.0	4.0–11.0	4.6–11.0	4.5–12.0	5.0–7.5	5.0–7.5	5.2–7.5
Number of points	43	43	49	44	62	37	37	48
R factor	–	–	–	–	–	0.057	0.043	0.036
SD (mV)	2.76	2.71	0.45	1.13	2.16	–	–	–

Note: NI – not included.

$Pb(OH)_2$ is predicted at pH *ca.* 8.2, which was not observed. This is additional evidence of the formation of $PbL_x(OH)_y$ species.

In order to provide more information about the model and the stability constants, additional experiments, performed by GEP, were done. In the course of the GEP titrations, precipitation was observed and only data recorded up to pH 7.5 was analyzed. Due to the precipitation restrictions, species expected to be formed at higher pH values, $PbL_2(OH)_y$, could not be included in the model to be refined. However, figure 5(A) shows that Z_M function builds up to 1, with no signs of halting at this value, which suggests formation of $PbL_2(OH)_y$ species. Upon refinement, model I fitted well with the experimental data, except for higher pA values, which correspond to pH values around 6.0, where the calculated Z_M values were lower than those recorded experimentally. This suggests formation of another metal complex, and this species should be PbHL since at pH 6, BTP occurs totally protonated as H_2L. After including PbHL in the refinement operations, model II was able to fit the experimental data, as can be seen in figure 5(A) and in table 2. Nevertheless, just like in DCP titrations, PbHL should not be a major species as it did not change significantly the overall stability constants of the other refined species. From both $[L_T] : [Pb_T]$ ratios 4 and 8, data were consistently refined in such a manner that the values obtained were in good agreement for both ratios.

When we compare the overall stability constants refined using model II for all $[L_T] : [Pb_T]$ ratios by both techniques (table 2), all values are in agreement. Thus, taking into account all refinements described above, the final model proposed for the Pb-BTP system includes PbHL, PbL, PbL_2, $PbL_2(OH)$, and $PbL_2(OH)_2$. Considering all the DCP and GEP titrations refined for model II (table 2), the final overall stability constants are listed in table 3.

To test this model, species distribution diagrams (SDDs), made using the final stability constant values (table 3) for experimental conditions used in DCP ($[L_T] : [Pb_T] = 100$, $[Pb_T] = 1 \times 10^{-5}$ M) and GEP ($[L_T] : [Pb_T] = 4$, $[Pb_T] = 1 \times 10^{-3}$ M), are presented in figure 6. From analysis of figure 6(A) (DCP conditions), it is possible to see that PbHL forms in little extension and almost simultaneously with PbL, which is in accord with our previous observations. For the lower ratio [figure 6(B)], the quantity of PbHL formed is larger, which explains the easier refinement (lower standard deviation) of this species from the GEP experiments. From figure 6(A), we see that complexation begins at about pH 6.5, which is in line with the $E_{1/2}$ *versus* pH plot although the effects are not clearly visible until pH 7, where the concentration of metal complexes reaches about 20% of the total metal concentration. From pH 7–8, we can see that PbL is the major species present with lesser amounts

Table 3. Overall stability constants for lead(II) or cadmium(II) complexes with BTP obtained in this work, after combining all polarographic and potentiometric results, at 25 °C and 0.1 M KNO_3 ionic strength.

Equilibrium	Pb(II)[a]	Cd(II)[b]
$M + L + H \rightleftharpoons HL$	11.4 ± 0.3	10.9 ± 0.4
$M + L \rightleftharpoons L$	4.7 ± 0.3	4.10 ± 0.07
$M + L + OH \rightleftharpoons L(OH)$	–	8.2 ± 0.2
$M + L + 2OH \rightleftharpoons L(OH)_2$	–	10.9 ± 0.2
$M + 2L \rightleftharpoons L_2$	8.8 ± 0.2	–
$M + 2L + OH \rightleftharpoons L_2(OH)$	14.4 ± 0.3	–
$M + 2L + 2OH \rightleftharpoons L_2(OH)_2$	18.4 ± 0.3	–

[a]403 Experimental points from eight independent titrations.
[b]592 Experimental points from eight independent titrations.

of PbL_2 and Pb(OH) species. This behavior is in agreement with the GEP data [figure 6(B)], as Z_M function increases beyond 1 uniformly, indicating that, at some point, PbL and PbL_2 are formed at the same time. For the higher $[L_T] : [Pb_T]$ ratio [figure 6(A)], between pH 8.5–10, $PbL_2(OH)$ is a major species in the system, being present in a fairly large quantity (more than 70%); these results are in agreement with the observations done in the $E_{1/2}$ *versus* pH plot [figure 3(A)], where the experimental slope is almost the same as the theoretical one (−52.8 *vs.* −58.5 mV per pH unit). For pH values higher than 10, there is a mixture of $PbL_2(OH)$ and $PbL_2(OH)_2$, where $PbL_2(OH)_2$ is, by far, the major complex in the system. This would indicate the formation of a slope of about −58.5 mV per pH unit as well. However, at pH 9.5, a smaller slope can be detected that may be related to the transitional presence of $PbL_2(OH)$; at this pH range, $PbL_2(OH)$ reaction only involves one proton, as one can see in reaction 8, and thus, a slope of 29.2 mV per pH unit is generated.

$$ML_2(OH) + H + 2e \leftrightarrow M(Hg) + 2L + H_2O \tag{8}$$

Finally, using the SDD data, we can calculate the predicted slope at each pH for a given mixture of species using the following equation:

$$S = \sum \%_a \left(\sum (\%_{H_xL_y} \times S_{a/H_xL_y}) \right) \tag{9}$$

where a stands for the species present in the system and S_{a/H_xL_y} represents the theoretical slope for a forming H_xL_y. Once all points have been estimated, we can calculate the averages for the considered pH ranges in the $E_{1/2}$ *versus* pH plot and compare them. The calculated slopes were 24.7 and 52.3 mV per pH unit, within 10% or less of the experimental values shown in figure 3(A) and strongly support the final model. Furthermore, these calculations also predict the decrease of the slope observed at pH around 9.5.

3.3. *Complexation studies of the Cd-BTP system*

From the analysis of the DCP titrations, performed at $[L_T] : [Cd_T] = 300$ and $[L_T] : [Cd_T] = 350$ ratios in the pH range between 4.0 and 11.0, only one DC wave was recorded, which moved to more cathodic values in the progress of the titrations. Thus, the Cd-BTP system behaves as labile throughout the experiments [15]. Since all titrations have similar behavior, only one of the titrations, performed at $[L_T] : [M_T] = 350$, will be discussed below in detail.

Analysis of the graphic $E_{1/2}$ *versus* pH [figure 3(C)] reveals three different regions. In region I (pH values below 7.2), where a slight shift was observed for pH values higher than 6.9, the main form of the ligand is H_2L; so, as predicted by equation (2), CdHL is likely to be formed albeit in low quantities. Continuing to region II, a slope of −19.5 mV per pH unit can be drawn. Since up to pH 9, the main form of the ligand is HL^- and the magnitude of the experimental slope is related to the theoretical one (−29.6 mV per pH unit) typical of one proton reactions, one can predict that CdL and Cd(OH) species are present in this region according to reactions 1 and 3, respectively. Like in the previous system, the lower experimental slope compared to the theoretical one may be representative of a species or a mixture of different species which is not fully formed. No formation of CdL_2 is predicted; according to reaction 4, formation of CdL_2 would generate a slope of about −59.2 mV per pH unit, which was not observed. This observation is also corroborated by the analysis of the $E_{1/2}$ *versus* pL plot [figure 3(D)], where only a slope of −23.4 mV per pL unit can be drawn.

Table 4. Refinement of the stability constants (as $\log_{10} \beta$) for the Cd-BTP system determined by DCP and GEP at 25 °C and ionic strength of 0.1 M KNO_3.

	DCP					GEP
$[L_T] : [Cd_T]$	350		350	300	300	4
$[Cd_T]$ (M)	1×10^{-5}		1×10^{-5}	1×10^{-5}	1×10^{-5}	1×10^{-3}
Complex	Model I	Model II	Model II	Model II	Model II	Model II
CdHL	NI	11.22 ± 0.06	10.92 ± 0.12	11.09 ± 0.08	10.33 ± 0.31	10.65 ± 0.02
CdL	4.19 ± 0.01	4.15 ± .0.01	4.04 ± 0.02	4.14 (fixed)	4.05 ± 0.01	4.082 ± 0.002
CdLOH	8.10 ± 0.03	8.07 ± 0.07	8.50 ± 0.02	8.17 ± 0.02	8.11 ± 0.04	NI
$CdL(OH)_2$	10.94 ± 0.02	11.3 ± 0.1	10.8 ± 0.1	10.66 ± 0.08	10.87 ± 0.09	NI
pH range	4.6–10.2	4.6–10.2	3.8–10.0	3.6–10.1	5.6–10.2	5.9–8.5
Number of points	44	44	36	43	36	109
R factor	–	–	–	–	–	0.006
SD (mV)	2.76	0.39	0.56	0.84	1.41	–

Note: NI – not included.

From figure 3(C), for pH values above 9.1, two distinct slopes can be drawn: one in region II (from pH 9.1 to 9.9) and another one in region III (from pH 10 to 10.8) of −19.5 and −38.3 mV per pH unit, respectively. These experimental slopes are lower than the theoretical ones (−29.6 and −59.2 mV per pH unit, respectively) involving formation of CdL(OH) and $CdL(OH)_2$ species, respectively. Above pH 9.1, L^{2-} is the dominant form of the ligand. So, for this range of pH, only reactions involving formation of $CdL(OH)_y$ species [equation (7)], where the number of protons involved are solely related to the number of hydroxide groups in the complex, can explain the experimental slopes observed.

Graphical analysis of the data obtained from DCP experiments pointed to a model based on $CdHL(OH)_y$ species (y = 0, 1, 2). Thus, the refinement operations of the stability constants for the Cd-BTP system were carried out assuming the following two models:

(1) CdL, CdL(OH), and $CdL(OH)_2$
(2) CdHL, CdL, CdL(OH), and $CdL(OH)_2$

For $[L_T] : [Cd_T]$ = 350, stability constants, refined for both models, are presented in table 4. Refinement operations, using model II, show a better fit to the experimental data, especially between pH 6.5 and 7.1 [see enlargement in figure 4(B)], due to the inclusion of CdHL. As for Pb-BTP, the refined values for the other species did not change significantly between models I and II, which suggest that these species should be major ones. For the other $[L_T] : [Cd_T]$ ratios, assuming model II, similar refined values for CdHL, CdL, CdL(OH), and $CdL(OH)_2$ species were obtained (table 4). Again, like previously for the Pb(II)-BTP system, the model containing only cadmium hydroxide complexes was added for comparative purposes. The difference between ECFC [unfilled dots in figure 4(B)] and CCFC for the $Cd_x(OH)_y$ species alone [small filled dots in figure 4(B)] clearly indicates strong complexation between Cd and BTP.

Additionally, GEP titrations were carried out, as described above, and the results obtained for $[L_T] : [Cd_T]$ = 4 are discussed here. As, in the course of the titrations, precipitation was observed, only data recorded up to pH 8.5 were included in the refinement operations. By analyzing the Z_M *versus* pL plot [figure 5(B)], it is possible to observe that a shift from $Z_M = 0$ occurs at pL = 6 (pH 6.25) presenting a rather shallow slope at the beginning increasing in steepness as we move to pL = 3.25 (about pH 8.5), where the experimental Z_M reaches 1; since the pH range is limited, due to precipitation, no further conclusions can

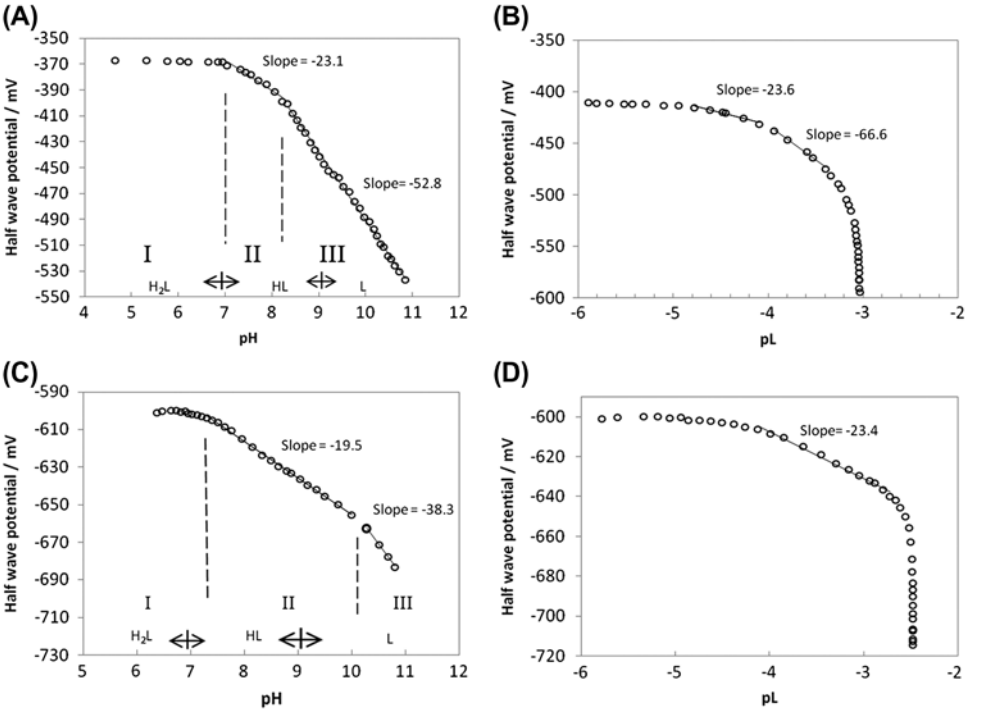

Figure 3. DCP experimental recorded potential as a function of pH at 25 °C and 0.1 M KNO_3 ionic strength for (A) Pb-BTP-OH system, $[L_T] : [Pb_T] = 100$, $[Pb_T] = 1 \times 10^{-5}$ M and (C) Cd-BTP-OH system, $[L_T] : [Cd_T] = 100$, $[Cd_T] = 1 \times 10^{-5}$ M. (B), (D) Half-wave potential as a function of free ligand concentration for the same Pb-BTP and Cd-BTP systems, respectively.

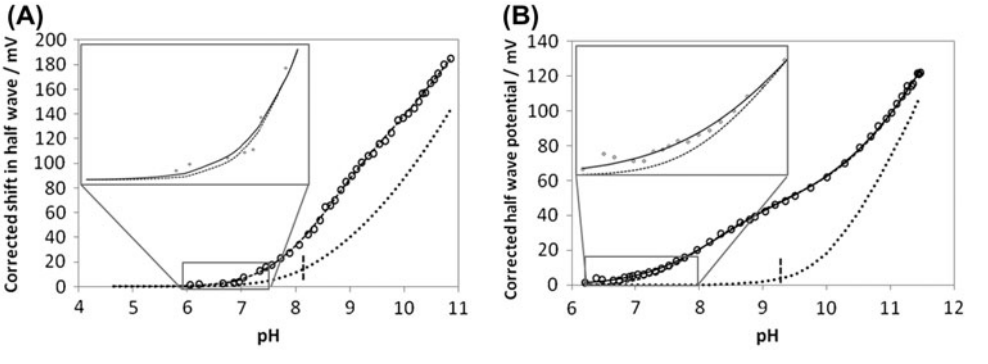

Figure 4. Corrected half-wave potential as a function of pH for (A) Pb-BTP and (B) Cd-BTP systems, respectively, from the DCP data recorded in figure 3. Unfilled dots (○) represent the experimental data, the dashed (- - -) and solid (—) lines represent models I and II, respectively, described in tables 2 and 4 for Pb-BTP and Cd-BTP systems, respectively. Small filled dots (…) represent the model with only $M(OH)_x$ species present in the system, where the vertical dashed line represents the pH where precipitation would occur if only $M(OH)_x$ species would be present.

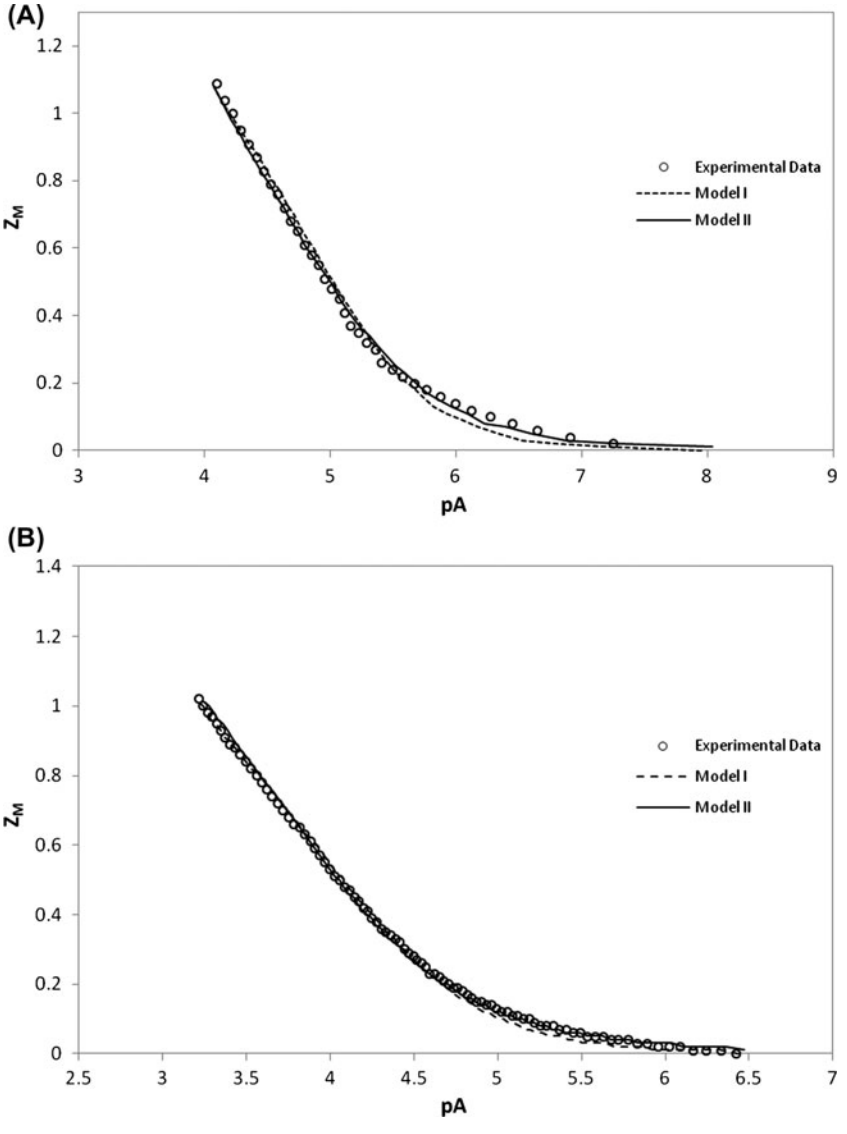

Figure 5. Z_M function calculated from the refinement operations performed on the GEP data by the program ESTA for (A) Pb-BTP system with $[L_T] : [Pb_T] = 4$, $[Pb_T] = 1 \times 10^{-3}$ M and (B) Cd-BTP system with $[L_T] : [Cd_T] = 4$, $[Cd_T] = 1 \times 10^{-3}$ M. Represented models can be found in tables 2 and 4, respectively.

be made. These observations support model II with CdHL, CdL, and possibly CdLOH as this model fits well with the experimental data, as shown in figure 5(B) and table 4.

From the discussion above, the final model proposed includes CdHL, CdL, CdL(OH), and $CdL(OH)_2$, and the final overall stability constants, considering all refined values from DCP and GEP titrations, are provided in table 3.

To test this model, SDDs were generated for DCP ($[L_T] : [Cd_T] = 350$, $[Cd_T] = 1 \times 10^{-5}$ M) and GEP ($[L_T] : [Cd_T] = 4$, $[Cd_T] = 1 \times 10^{-3}$ M) [figure 6(C) and (D), respectively] conditions using the values presented in table 3. From the analysis of

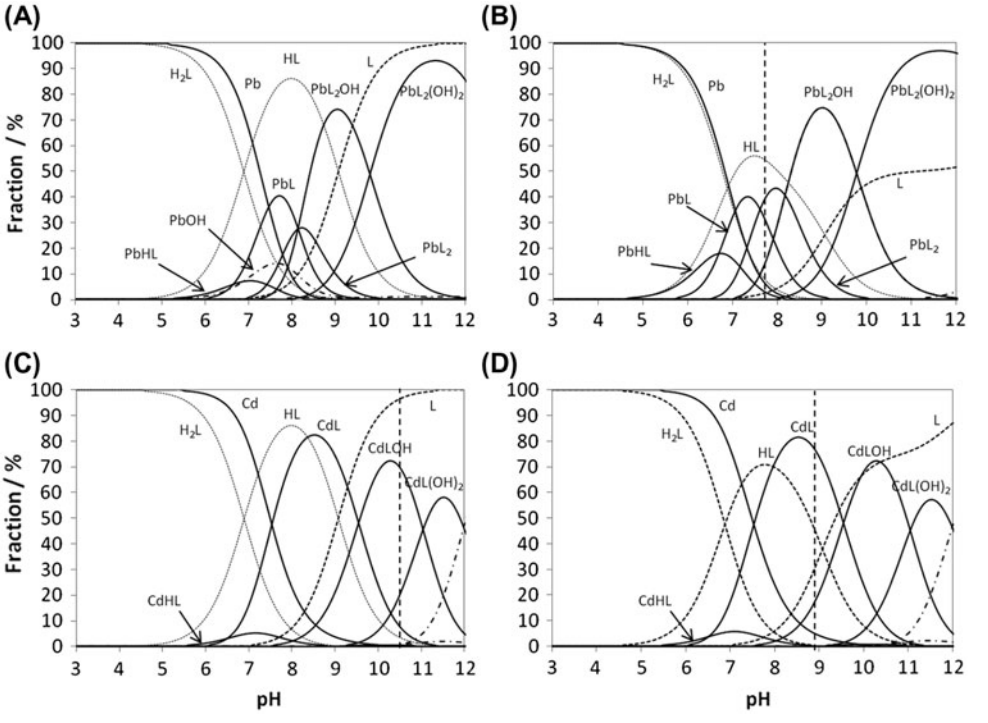

Figure 6. SDDs for the final M-BTP models described in table 3: (A, B) Pb-BTP-$(OH)_x$, and (C, D) Cd-BTP-$(OH)_x$ systems. (A) $[L_T]:[Pb_T] = 100$, $[Pb_T] = 1 \times 10^{-5}$ M; (B) $[L_T]:[Pb_T] = 4$, $[Pb_T] = 1 \times 10^{-3}$ M; (C) $[L_T]:[Cd_T] = 350$, $[Cd_T] = 1 \times 10^{-5}$ M; and (D) $[L_T]:[M_T] = 4$, $[Cd_T] = 1 \times 10^{-3}$ M. Dashed vertical lines represent precipitation events. Alternating dashed lines represent $M(OH)_x$ species. For sake of simplicity, charges were omitted.

figure 6(C), we can see that CdL is the major species present in the system throughout a large pH range (from 7.5 to 9.5); however, other species are present, CdHL and CdL(OH). This mixture and the inability of the species to be fully formed explains why the theoretical value is not achieved, in line with the observations from the half-height potential *versus* pH plot [figure 3(C)]. Before pH 7.5, we can see formation of CdHL, although in very low quantities, which explains the small shift in $E_{1/2}$ before this pH [figure 3(C)]. After pH 9, the major species present is CdL(OH), which is always mixed with CdL, and this is the reason why the slope obtained [figure 3(C)] is lower than the theoretical one (−29.6 mV per pH unit). Around pH 10, $CdL(OH)_2$ starts to be formed, forming a mixture constituted by 60% and 20% of CdL(OH) and $CdL(OH)_2$, respectively; these results explain the slope observed experimentally [figure 3(C)], which is between the theoretical slopes of the reactions involving one and two protons. Finally, the SDD predicts precipitation at pH 10.7, in agreement with what was observed experimentally (data not shown).

For $[L_T]:[Cd_T] = 4$ [figure 6(D)], CdL is the major species present, while CdHL and CdL(OH) species are present in lower quantities. Experimentally, precipitation was observed at pH 8.8, which is in agreement with SDD.

Finally, using equation (9), it is possible to calculate the theoretical slope for each pH of a given mixture of species and compare it with the experimental data. For the same pH

ranges considered in figure 3(C), the calculated slopes were −20.0 and −42.9 mV per pH unit, while the experimental values were −19.5 and −38.3 mV per pH unit, respectively. These results show that experimental slopes are within 10% of the calculated ones, which strongly supports the refined model.

3.4. *NMR data*

In order to corroborate the complexation between Pb(II) and BTP, ^{1}H NMR experiments of Pb-BTP at $[L_T]:[Pb_T] = 2$ with a $[Pb_T] = 1 \times 10^{-4}$ M were conducted at pH 3.0 and 7.5 and compared with the ^{1}H NMR spectra recorded for the ligand at the same concentration and pH. Under these conditions, SDDs predicted no complexation at pH 3 and formation of 14.4%, of PbL (data not shown) at pH 7.5. At pH 3, the ^{1}H NMR spectra of the ligand show three well-defined signals (a singlet, a triplet, and a quintuplet), in which chemical shifts corresponding to the protons are marked as *c*, *b,* and *a*, respectively, in the structure of BTP presented in figure 1. At pH 7.5, the ^{1}H NMR spectra of the Pb-BTP system show a downfield shift of the signal of the triplet (in figure 1, corresponds to the protons marked as *b*) compared to that of the free ligand at the same pH (data not shown). Even though this shift is small (about 0.09 ppm), explained by the small amount of complex (about 8%) present in solution when compared with the total amount of BTP, it clearly supports the complex formation between lead and BTP.

3.5. *Evaluation of the stability constants*

A comparison of the stability constant values refined in this work for Cd-BTP (log $\beta_{CdL} = 4.10$) and Pb-BTP (log $\beta_{PbL} = 4.7$) with those of NH_3 (log $\beta_{Cd\text{-}NH3} = 2.56$ and log $\beta_{Pb\text{-}NH3} = 1.55$ [14]) shows that BTP has greater complexing capabilities than NH_3 and suggests that BTP does not behave as a monodentate, but instead, as a bidentate ligand. An analysis of the structure of BTP also points in this way since this ligand has two possible sites for coordination, at both secondary amines. The comparison of log $\beta_{CdL(OH)} = 8.2$ with the theoretical one [CdL(OH) = CdL + Cd(OH) = 4.10 + 3.77 = 7.87] shows that they are very similar. The same behavior is observable with log $\beta_{PbL2(OH)}$ (14.4 *vs.* 14.70). However, the comparison between the log $\beta_{CdL(OH)2}$, 10.9, and log $\beta_{PbL2(OH)2}$, 18.4, with the theoretical values [$ML_x(OH)_2 = ML_x + M(OH)_2$; Cd: 4.10 + 7.10 = 11.20; Pb: 8.8 + 10.40 = 19.2]

Table 5. Comparison between ML complex stability constants and number of alkyl groups bounded to the nitrogen for some biological buffers and other amines.

Ligand	β_{CdL}^{Cd+L}	β_{PbL}^{Pb+L}	Alkyl groups bound to *N*	Refs.
Ammonia	2.56	1.55	0	[14]
Ethylenediamine	5.4	5.05	1	[14]
Trimethylenediamine	4.5	**8.16***	1	[14]
BTP	4.1	4.78	2	This work
TAPS	2.5	3.27	2	[19, 20]
AMPSO	2.1	2.9	2	[21, 22]
Bis-Tris	2.47	4.32	3	[14]
DIPSO	2.9	3.4	3	[19, 21]
EDTA	16.5	18	3	[14]

*PbL_2 instead of PbL.

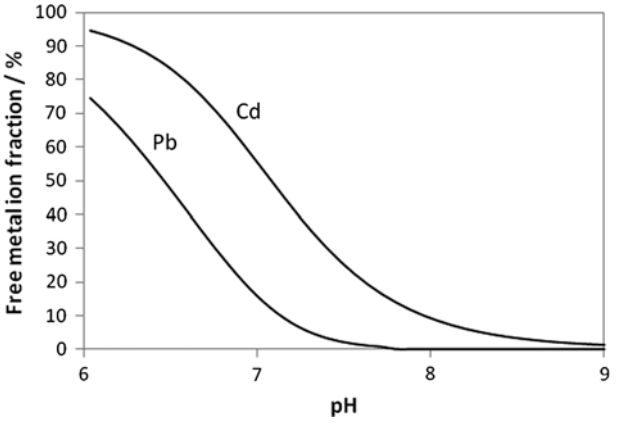

Figure 7. Variation of the free metal *vs.* pH for M-BTP systems. Chemical speciation calculations were performed assuming final models described in table 3 and $[L_T] : [M_T] = 1000$, $[M_T] = 1 \times 10^{-5}$ M.

shows some slight differences. These differences may be related to the different mechanisms of ML_x hydrolyses, as the proton may be lost from either the coordinating water molecules or the ligand itself, and the stability constant will be different in both cases [17]. Analogous behaviors have been reported for other zwitterionic ligands, such as TAPSO [8], AMPSO [11], and DIPSO [18]. It is not possible, however, based on potentiometric and/or polarographic data, to determine the structure or the type of bonds of the complexes formed.

When comparing both metal systems, some differences are obvious; both systems have different models and, in general, Pb(II) presents higher stability constant values. This can be explained by the differences of the metal properties and how these metal ions interact differently with ligands with amine groups. If we look at NH_3 stability constants, Cd(II) presents a larger stability constant in comparison with Pb(II). The same is true for other ligands with primary amine groups such as ethylenediamine and trimethylenediamine (table 5). But, as we move from primary to tertiary amines, the larger stability constants are found in Pb(II) complexes because the increasing number of alkyl groups on the amine increases its basicity and thus favors the larger and "harder" Pb(II) ion [23] (table 5). BTP has two secondary amines in its structure that are responsible for its coordination properties; therefore, this ligand has an intermediary basicity, which may reflect the slightly higher stability constants of Pb(II) in comparison with Cd(II). Finally, the value found for PbL_2 in the Pb(II) system is not as large as expected ($PbL + PbL = PbL_2$; $4.7 + 4.7 = 9.4$), which may be a consequence of the steric hindrance from the hydroxymethyl groups of the molecule. However, due to the "harder" character and larger ionic radii of Pb(II), this metal ion is able to overcome this hindrance and form ML_2 species while Cd(II) does not.

For biological studies, where BTP is often used, this study indicates that BTP forms strong complexes with both Pb(II) and Cd(II). Based on the Cd(II) and Pb(II) concentrations, usually used in toxicological studies, from 1×10^{-6} to 1×10^{-4} M and 1×10^{-7} to 1×10^{-5} M [24–30], respectively, and the usual concentrations suggested by BTP suppliers (1×10^{-1} to 1×10^{-2} M), SDDs were made with $[L_T] = 1 \times 10^{-2}$ M, $[M_T] = 1 \times 10^{-5}$ M (figure 7). From this figure, it is possible to witness, for both systems, a significant decrease in the free metal ion concentrations within the pH buffer range, especially in the case of Pb (II), where a very low free metal ion is present from pH 8 onward.

Funding

This work is financed by FEDER funds through Programa Operacional Factores de Competitividade – COMPETE and by National Funds through FCT – Fundação para a Ciência e a Tecnologia in the ambit of project Pest-C/EQB/LA0006/2013. The authors thank Prof. Ignacy Cukrowski from the University of Pretoria (South Africa) for polarographic modeling software (3D-CFC program) and Prof. Carlos Gomes from the Faculty of Sciences/Porto University for the COPOTISY program.

References

[1] M.-L. Hu, A. Morsali, L. Aboutorabi. *Coord. Chem. Rev.*, **255**, 2821 (2011).
[2] D.M. Templeton, Y. Liu. *Chem. Biol. Interact.*, **188**, 267 (2010).
[3] Directive 2002/95/EC Of the european parliament and of the council of 27 January 2003 on the restriction of the use of certain hazardous substances in electrical and electronic equipment. *Off. J. Eur. Union*, **L37**, 19 (2003).
[4] N.E. Good, G.D. Winget, W. Winter. *Biochemistry*, **5**, 467 (1966).
[5] W.J. Ferguson, K.I. Braunschweiger, W.R. Braunschweiger, J.R. Smith, J.J. McCormick, C.C. Wasmann, N.P. Jarvis, D.H. Bell, N.E. Good. *Anal. Biochem.*, **104**, 300 (1980).
[6] T. Laureys, I.S.S. Pinto, C.V.M. Soares, H.B. Boppudi, H.M.V.M. Soares. *J. Chem. Eng. Data*, **57**, 87 (2012).
[7] K.S. Bai, K.H. Hong. *Bull. Korean Chem. Soc.*, **21**, 650 (2000).
[8] C.M.M. Machado, I. Cukrowski, P. Gameiro, H.M.V.M. Soares. *Anal. Chim. Acta*, **493**, 105 (2003).
[9] A.J. Bard, L.R. Faulkner. *Electrochemical Methods: Fundamentals and Applications*, 2nd Edn, John Wiley & Sons, New York (2000).
[10] I. Cukrowski. *Anal. Chim. Acta*, **336**, 23 (1996).
[11] C.M.M. Machado, I. Cukrowski, H.M.V.M. Soares. *Helv. Chim. Acta*, **86**, 3288 (2003).
[12] P.M. May, K. Murray, D.R. Williams. *Talanta*, **35**, 825 (1988).
[13] P.M. May, K. Murray, D.R. Williams. *Talanta*, **32**, 483 (1985).
[14] A.E. Martell, R.M. Smith. *NIST Standard Reference Database 46 (Version 8.0)* US Department of Commerce, National Institute of Standards and Technology, Washington, DC (2004).
[15] I. Cukrowski, R.D. Hancock, R.C. Luckay. *Anal. Chim. Acta*, **319**, 39 (1996).
[16] I. Cukrowski, F. Marsicano, R.D. Hancock. *Polyhedron*, **14**, 1661 (1995).
[17] I. Granberg, W. Forsling, S. Sjöberg. *Acta Chem. Scand.*, 36a, 819 (1982).
[18] C.M.M. Machado, S. Scheerlinck, I. Cukrowski, H.M.V.M. Soares. *Anal. Chim. Acta*, **518**, 117 (2004).
[19] C.M.M. Machado, G.M.S. Alves, I.S.S. Pinto, S. Scheerlinck, S. Van Acker, H.M.V.M. Soares. *J. Solution Chem.*, **42**, 1602 (2013).
[20] C.M.M. Machado, O. Victoor, H.M.V.M. Soares. *Talanta*, **71**, 1326 (2007).
[21] M. Eliat-Eliat, I.S.S. Pinto, G.M.S. Alves, V. Olle, H.M.V.M. Soares. *J. Coord. Chem.*, **66**, 3544 (2013).
[22] C.M.M. Machado, I. Cukrowski, H.M.V.M. Soares. *Electroanalysis*, **18**, 719 (2006).
[23] S. Canepari, V. Carunchio, P. Castellano, A. Messina. *Talanta*, **47**, 1077 (1998).
[24] F.D. Ledda, P. Ramoino, S. Ravera, E. Perino, P. Bianchini, A. Diaspro, L. Gallus, R. Pronzato, R. Manconi. *Aquat. Toxicol.*, 140–141, 98 (2013).
[25] P.M. Kopittke, F.P.C. Blamey, C.J. Asher, N.W. Menzies. *J. Exp. Bot.*, **61**, 945 (2010).
[26] X. Chen, G. Wang, X. Li, C. Gan, G. Zhu, T. Jin, Z. Wang. *Food Chem. Toxicol.*, **60**, 530 (2013).
[27] D. Alsop, C.M. Wood. *Aquat. Toxicol.*, **140–141**, 257 (2013).
[28] A.V. Ivanina, E. Beniash, M. Etzkorn, T.B. Meyers, A.H. Ringwood, I.M. Sokolova. *Aquat. Toxicol.*, **140–141**, 1231 (2013).
[29] R. Flouty, G. Estephane. *J. Environ. Manage.*, **111**, 106 (2012).
[30] Y. Yang, X.S. Lu, D.L. Li, Y.J. Yu. *Biomed. Environ. Sci.*, **26**, 474 (2013).